

LETTER • OPEN ACCESS

## Interannual variation of reactive nitrogen emissions and their impacts on PM<sub>2.5</sub> air pollution in China during 2005–2015

To cite this article: Youfan Chen *et al* 2021 *Environ. Res. Lett.* **16** 125004

View the [article online](#) for updates and enhancements.

You may also like

- [New ammonia demand: ammonia fuel as a decarbonization tool and a new source of reactive nitrogen](#)  
Kazuya Nishina
- [Global, regional and national trends of atmospheric ammonia derived from a decadal \(2008–2018\) satellite record](#)  
Martin Van Damme, Lieven Clarisse, Bruno Franco *et al.*
- [Nitrogen footprints: past, present and future](#)  
James N Galloway, Wilfried Winiwarter, Adrian Leip *et al.*

ENVIRONMENTAL RESEARCH  
LETTERS

## LETTER

## OPEN ACCESS

## RECEIVED

31 August 2021

## REVISED

20 October 2021

## ACCEPTED FOR PUBLICATION




4 November 2021

## PUBLISHED

19 November 2021

Original content from this work may be used under the terms of the [Creative Commons Attribution 4.0 licence](#).

Any further distribution of this work must maintain attribution to the author(s) and the title of the work, journal citation and DOI.

Interannual variation of reactive nitrogen emissions and their impacts on PM<sub>2.5</sub> air pollution in China during 2005–2015Youfan Chen<sup>1,2</sup>, Lin Zhang<sup>1,\*</sup> , Daven K Henze<sup>3,\*</sup>, Yuanhong Zhao<sup>4</sup>, Xiao Lu<sup>5</sup> , Wilfried Winiwarter<sup>6,7</sup> , Yixin Guo<sup>1</sup>, Xuejun Liu<sup>8</sup>, Zhang Wen<sup>8</sup>, Yuepeng Pan<sup>9</sup> and Yu Song<sup>10</sup>

<sup>1</sup> Laboratory for Climate and Ocean-Atmosphere Studies, Department of Atmospheric and Oceanic Sciences, School of Physics, Peking University, Beijing 100871, People's Republic of China

<sup>2</sup> Sichuan Academy of Environmental policy and planning, Chengdu, Sichuan 610041, People's Republic of China

<sup>3</sup> Department of Mechanical Engineering, University of Colorado Boulder, Boulder, CO 80309, United States of America

<sup>4</sup> College of Oceanic and Atmospheric Sciences, Ocean University of China, Qingdao 266100, People's Republic of China

<sup>5</sup> School of Atmospheric Sciences, Sun Yat-sen University, Zhuhai, Guangdong 519082, People's Republic of China

<sup>6</sup> International Institute for Applied Systems Analysis (IIASA), Laxenburg, Austria

<sup>7</sup> The Institute of Environmental Engineering, University of Zielona Góra, Zielona Góra, Poland

<sup>8</sup> Beijing Key Laboratory of Farmland Soil Pollution Prevention and Remediation, College of Resources and Environmental Sciences, China Agricultural University, Beijing 100193, People's Republic of China

<sup>9</sup> State Key Laboratory of Atmospheric Boundary Layer Physics and Atmospheric Chemistry (LAPC), Institute of Atmospheric Physics, Chinese Academy of Sciences, Beijing 100029, People's Republic of China

<sup>10</sup> State Key Joint Laboratory of Environmental Simulation and Pollution Control, Department of Environmental Science, Peking University, Beijing 100871, People's Republic of China

\* Authors to whom any correspondence should be addressed.

E-mail: [zhanglg@pku.edu.cn](mailto:zhanglg@pku.edu.cn) and [daven.henze@colorado.edu](mailto:daven.henze@colorado.edu)

**Keywords:** reactive nitrogen, ammonia, air pollution, satellite observations, fine particulate matter, emission inversion

Supplementary material for this article is available [online](#)

**Abstract**

Emissions of reactive nitrogen as ammonia (NH<sub>3</sub>) and nitrogen oxides (NO<sub>x</sub>), together with sulfur dioxide (SO<sub>2</sub>), contribute to formation of secondary PM<sub>2.5</sub> in the atmosphere. Satellite observations of atmospheric NH<sub>3</sub>, NO<sub>2</sub>, and SO<sub>2</sub> levels since the 2000s provide valuable information to constrain the spatial and temporal variability of their emissions. Here we present a bottom-up Chinese NH<sub>3</sub> emission inventory combined with top-down estimates of Chinese NO<sub>x</sub> and SO<sub>2</sub> emissions using ozone monitoring instrument satellite observations, aiming to quantify the interannual variations of reactive nitrogen emissions in China and their contributions to PM<sub>2.5</sub> air pollution over 2005–2015. We find small interannual changes in the total Chinese anthropogenic NH<sub>3</sub> emissions during 2005–2016 (12.0–13.3 Tg with over 85% from agricultural sources), but large interannual change in top-down Chinese NO<sub>x</sub> and SO<sub>2</sub> emissions. Chinese NO<sub>x</sub> emissions peaked around 2011 and declined by 22% during 2011–2015, and Chinese SO<sub>2</sub> emissions declined by 55% in 2015 relative to that in 2007. Using the GEOS-Chem chemical transport model simulations, we find that rising atmospheric NH<sub>3</sub> levels in eastern China since 2011 as observed by infrared atmospheric sounding interferometer and atmospheric infrared sounder satellites are mainly driven by rapid reductions in SO<sub>2</sub> emissions. The 2011–2015 Chinese NO<sub>x</sub> emission reductions have decreased regional annual mean PM<sub>2.5</sub> by 2.3–3.8 μg m<sup>-3</sup>. Interannual PM<sub>2.5</sub> changes due to NH<sub>3</sub> emission changes are relatively small, but further control of agricultural NH<sub>3</sub> emissions can be effective for PM<sub>2.5</sub> pollution mitigation in eastern China.

**1. Introduction**

Nitrogen (N) is an essential element for life, but most N in the Earth cannot be used directly by ecosystems. The productivity of the ecosystem depends on the

abundance of reactive N (Nr or fixed N) (Vitousek *et al* 2002). Excessive reactive N will, however, induce negative environmental effects, such as causing soil acidification, eutrophication, decreasing the diversity of ecosystems (Galloway 2001, Galloway *et al* 2003),

and increasing nitric oxide (NO) and nitrous oxide (N<sub>2</sub>O) emissions contributing to air pollution and global warming (Pilegaard *et al* 2006, Eickenscheidt *et al* 2011). China is one of the regions with the most intensive reactive nitrogen emissions in the globe due to its rapid industrialization, urbanization, as well as high demand for food production (Liu *et al* 2013). Recent satellite observations have recorded significant changes in atmospheric ammonia (NH<sub>3</sub>) and nitrogen dioxide (NO<sub>2</sub>) levels over China since the 2000s (Qu *et al* 2017, van der A *et al* 2017, Warner *et al* 2017, Liu *et al* 2018a). Here we will use these satellite observations to constrain Nr emissions in China over 2005–2015 and to assess their impacts on the PM<sub>2.5</sub> air quality.

Emissions of Nr to the atmosphere are mainly in the forms of NH<sub>3</sub> and nitrogen oxides (NO<sub>x</sub> = NO + NO<sub>2</sub>). NH<sub>3</sub> is the most abundant alkaline gas in the atmosphere. Over 85% of NH<sub>3</sub> is emitted from agricultural activities (Huang *et al* 2012, Paulot *et al* 2014, Zhang *et al* 2018), including nitrogen fertilizer application to farmland (Sha *et al* 2021) and livestock husbandry systems (Bai *et al* 2016). Chemical industry, residential, human wastes, and traffic are other important anthropogenic sources (Kean and Harley 2000, Sun *et al* 2017). NH<sub>3</sub> can also be released from rewetting processes of natural soils (Hickman *et al* 2018). NO<sub>x</sub> is mainly emitted as a byproduct of combustion at high temperature, such as from industry and transportation sectors. Soil and lightning are natural sources of NO<sub>x</sub> (Boersma *et al* 2005, Ciais *et al* 2014). Both NH<sub>3</sub> and NO<sub>x</sub> are precursors of secondary aerosols. NH<sub>3</sub> in the atmosphere reacts with sulfuric acid (H<sub>2</sub>SO<sub>4</sub>; produced from the oxidation of SO<sub>2</sub>) and nitric acid (HNO<sub>3</sub>; produced from the oxidation of NO<sub>x</sub>) to form ammonium sulfate and ammonium nitrate aerosols.

Previous studies have shown that the SNA (sulfate–nitrate–ammonium) aerosols account for 20%–57% of PM<sub>2.5</sub> (particulate matter with an aerodynamic diameter less than 2.5 μm) in Chinese cities (Wang *et al* 2011, Huang *et al* 2014, Liu *et al* 2018b). Changes in Nr and SO<sub>2</sub> emissions can thus strongly affect the SNA fraction of PM<sub>2.5</sub>. Surface measurements have recorded large decreases in sulfate aerosol concentrations and weak decreases or even increases in nitrate aerosol levels over North China in recent years (Li *et al* 2019a, Zhai *et al* 2021), as driven by the recent clean air actions targeting emissions of SO<sub>2</sub>, NO<sub>x</sub>, and primary aerosols (Zheng *et al* 2018, Zhang *et al* 2019). NH<sub>3</sub> emissions have not been effectively regulated so far in China, and they have drawn increasing attentions for understanding their mitigation potentials and impacts on PM<sub>2.5</sub> air pollution (Liu *et al* 2019, Liu *et al* 2021, Guo *et al* 2020). For example, Liu *et al* (2019) reported that 50% NH<sub>3</sub> emission reductions combined with 15% reductions of SO<sub>2</sub> and NO<sub>x</sub> emissions could remove 11%–17% of the total PM<sub>2.5</sub> in China. Here we aim to understand

how interannual variations of Chinese NH<sub>3</sub> emissions might have contributed to changes in PM<sub>2.5</sub> concentrations over China in the recent past.

In this work, we extend our bottom-up estimates of Chinese NH<sub>3</sub> emissions (Zhang *et al* 2018) to the years 2005–2016, and we evaluate the GEOS-Chem model simulated atmospheric NH<sub>3</sub> concentrations against satellite NH<sub>3</sub> observations. Satellite observations of NO<sub>2</sub> and SO<sub>2</sub> columns are also applied to constrain the interannual variations of Chinese NO<sub>x</sub> and SO<sub>2</sub> emissions over this time period (2005–2015). We further quantify the changes of PM<sub>2.5</sub> concentrations in China contributed by the interannual changes in anthropogenic NH<sub>3</sub>, NO<sub>x</sub>, and SO<sub>2</sub> emissions, respectively, over 2005–2015 using the GEOS-Chem model simulations.

## 2. Model description and observations

### 2.1. The GEOS-chem model

Here we use GEOS-Chem v12.1.1 (<http://acmg.seas.harvard.edu/geos/>), a three-dimensional global chemical transport model to simulate the chemical and physical processes of Nr in the atmosphere from 2005 to 2015 in China. The model is driven by the MERRA-2 assimilated meteorological data provided by the Global Modeling and Assimilation Office at the National Aeronautics and Space Administration (NASA). Meteorology fields such as temperature, relative and specific humidity, vertical pressure velocity, and surface pressure have a temporal resolution of 3 h, and sea level pressure, tropopause pressure, and other surface variables are at 1 h resolution. The model has 47 vertical layers from surface to 0.01 hPa, and the lowest layer is centered at 58 m above sea level.

GEOS-Chem simulates a detailed tropospheric O<sub>3</sub>–NO<sub>x</sub>–hydrocarbon–aerosol–halogen chemistry as described by Park *et al* (2004) and Mao *et al* (2010). The chemistry system fully couples the H<sub>2</sub>SO<sub>4</sub>–HNO<sub>3</sub>–NH<sub>3</sub> inorganic aerosol thermodynamics system from the ISORROPIA-II thermodynamical model (Fountoukis and Nenes 2007). NH<sub>3</sub> preferably reacts with sulfuric acid to form ammonium bisulfate and ammonium sulfate, then excessive NH<sub>3</sub> would combine with nitric acid to form ammonium nitrate (Binkowski and Roselle 2003). NO<sub>x</sub> is also a precursor tropospheric ozone, affecting atmospheric oxidizing capacity and the formation of secondary organic aerosols (SOA). In this study we do not analyze SOA, and focus on the SNA components that are directly related to Nr emissions. Both Nr gases and aerosols deposit to the surface via wet deposition (convective scavenging and largescale precipitation) following the parameterization of Liu *et al* (2001) and dry deposition using a standard resistance-in-series model (Wesely 1989, Zhang *et al* 2001). The GEOS-Chem model simulation of Nr concentrations and deposition over China have been evaluated in a number of previous studies (Wang *et al* 2013, Zhang *et al* 2015, Zhang *et al* 2016,

Zhao *et al* 2015, Shao *et al* 2019, Lu *et al* 2021, Zhai *et al* 2021).

Emissions in GEOS-Chem v12.1.1 are processed through HEMCO (Harvard–NASA Emission Component) (Keller *et al* 2014). We used the Community Emissions Data System (Hoesly *et al* 2018) for global anthropogenic emissions, overwritten by regional emissions inventories including 2011 NEI (National Emissions Inventory) from EPA (United States Environmental Protection Agency) for US (NEI-2011), EMEP (European Monitoring and Evaluation Programme; [www.emep.int/index.html](http://www.emep.int/index.html)) emissions over Europe, and Canada's Air Pollutant Emissions Inventory. Emissions over Asia are overwritten by the MIX inventory (Li *et al* 2017) that includes the MEIC inventory (Multi-resolution Emission Inventory for China; <http://meicmodel.org/>) over China except for NH<sub>3</sub>, NO<sub>x</sub>, and SO<sub>2</sub> emissions in China as will be described below. Natural NO<sub>x</sub> sources from soil and lightning are also included (Lu *et al* 2021).

In this study we have conducted four sets of GEOS-Chem model simulations for 2005–2015 at the global 2° latitudes by 2.5° longitude resolution. The standard simulation (BASE) uses the emission setting as described above that accounts for the interannual variations of Chinese Nr and SO<sub>2</sub> anthropogenic emissions. Three sets of sensitivity simulations by fixing the Chinese anthropogenic NH<sub>3</sub>, Nr (NH<sub>3</sub> + NO<sub>x</sub>), and additionally SO<sub>2</sub> (Nr + SO<sub>2</sub>) emissions, respectively, to the year 2005 are conducted (i.e. FixNH<sub>3</sub>, FixNr, and FixALL), and their differences with the BASE simulation and with each other estimate the impacts from their emissions' interannual variations. For better evaluating the model results, we have also conducted a nested GEOS-Chem simulation using the BASE emission conditions for the years 2005–2015 at a higher 0.5° latitude × 0.625° longitude resolution over Asia and 2° latitudes × 2.5° longitude for the rest of the world. All the simulations are initiated after one year spin-up.

## 2.2. Observations

We have compiled an ensemble of surface and satellite observations to evaluate our estimates of Nr emissions and resulting model simulations. We use observed surface NH<sub>3</sub> concentration data at 53 sites for 2015 over China from AMoN-China (Pan *et al* 2018), measurements of sulfate, nitrate and ammonium aerosol concentrations from CAWNET (Zhang *et al* 2012) over 2006–2007 and from Zhang *et al* (2019) over 2013–2015. We also use wet deposition observations of ammonium and nitrate, including 57 sites from EANET from 2005 to 2015 (EANET 2005–2015), ten sites from the Regional Atmospheric Deposition Observation Network on the North China Plain (Pan *et al* 2012) during 2008–2010, and 43 sites from the Nationwide Nitrogen Deposition Monitoring Network (Xu *et al* 2015) during 2010–2012.

We use satellite observations of atmospheric NH<sub>3</sub> concentrations from the infrared atmospheric sounding interferometer (IASI) and the atmospheric infrared sounder (AIRS). IASI is passive infrared Fourier transform spectrometer aboard the MetOp-A satellite in a polar sun-synchronous orbit with equator crossing local time of 09:30 in the morning and 21:30 at night (Van Damme *et al* 2014). Here we use the level 2 dataset of Artificial Neural Network for IASI–NH<sub>3</sub>–v2.2 R-I (Van Damme *et al* 2017). Morning observations have lower relative errors than those at night, so that we only use morning data with relative errors less than 100%, and then apply the relative error weighted mean method (Van Damme *et al* 2014) to compute monthly mean observations on a 0.25° latitude × 0.25° longitude grid over 2008–2015. The AIRS instrument aboard the NASA's Aqua satellite platform provides atmospheric NH<sub>3</sub> retrievals since 2002 (Warner *et al* 2016). Here we use the AIRS NH<sub>3</sub> data at 918 hPa where the retrieval sensitivity peaks from September 2002 to August 2016 over China as presented by Warner *et al* (2016), Warner *et al* (2017).

We also use satellite observations of NO<sub>2</sub> and SO<sub>2</sub> columns from the ozone monitoring instrument (OMI). OMI aboard the NASA's Aura satellite launched in 2004 measures backscattered solar radiation with a nadir-scanning resolution of 13 × 24 km<sup>2</sup> and at local passing time of 13:45 (Levelt *et al* 2006). We use the NASA standard products of daily Level-3 NO<sub>2</sub> tropospheric column (Krotkov *et al* 2019; [https://disc.gsfc.nasa.gov/datasets/OMNO2d\\_003/summary?keywords=TROPOMI%20NO2](https://disc.gsfc.nasa.gov/datasets/OMNO2d_003/summary?keywords=TROPOMI%20NO2)) and SO<sub>2</sub> planetary boundary layer (PBL) column (Li *et al* 2020; [https://disc.gsfc.nasa.gov/datasets/OMSO2e\\_003/summary?keywords=OMSO2e](https://disc.gsfc.nasa.gov/datasets/OMSO2e_003/summary?keywords=OMSO2e)) for the period of 2005–2015. Both products have a spatial resolution of 0.25° × 0.25°, and are regridded to the model 2° × 2.5° resolution.

We further evaluate the model simulated surface PM<sub>2.5</sub> concentrations with available PM<sub>2.5</sub> datasets. We use the nationwide PM<sub>2.5</sub> surface measurements for 2013–2015 obtained from the China National Environmental Monitoring Center (CNEMC; <https://air.cnemc.cn:18007/>). Ground-level PM<sub>2.5</sub> products derived from satellite observations of aerosol optical depth over 2005–2015 are also applied (Hammer *et al* 2020; <https://sites.wustl.edu/acag/datasets/surface-pm2-5/#V4.CH.03>). The products have a spatial resolution of 0.1° × 0.1° and are regridded to 0.5° × 0.625°.

In addition, the land cover datasets retrieved from the moderate resolution imaging spectroradiometer (MODIS) aboard the Terra and Aqua satellites are applied to identify the changes of cropland distributions in China. We use the Terra-Aqua combined land cover product (MCD12Q1) (<https://modis-land.gsfc.nasa.gov/landcover.html>), in which



the types of land cover at 500 m resolution are identified to 17 classes, including 11 natural vegetation classes, three human-altered classes, and three non-vegetated classes. We extract the grids classified as cropland and calculate the cropland areas at the model  $0.5^\circ \times 0.625^\circ$  resolution. The MCD12Q1 products covers the period of 2005–2012, and the latest available year 2012 data is applied to the years afterwards in this study.

### 3. Results and discussion

#### 3.1. Estimates of Chinese NH<sub>3</sub> emissions over 2005–2016

Previously we have developed a bottom-up inventory of Chinese agricultural NH<sub>3</sub> emissions for the year 2008 (Zhang *et al* 2018). Here we extend the bottom-up estimates of Chinese agricultural NH<sub>3</sub> emissions to 2005–2016. Details of the bottom-up method can be found in Zhang *et al* (2018). Below we provide a brief summary and describe our improvements for estimating the interannual variations of Chinese NH<sub>3</sub> emissions over 2005–2016.

The NH<sub>3</sub> emissions from fertilizer use are based on practical fertilizer application information, including cropland area, fertilizer application timing and rate for 21 types of crops, vegetables, and fruits. Emission factors are calculated as a function of fertilizer type, application mode, soil pH, and soil cation exchange capacity, and further modulated by local surface temperature and wind speed. We previously used a baseline cropland area for the year 2000 (Zhang *et al* 2018). Here we scale the baseline cropland area to match those observed by MODIS as described in the section above to account for their interannual changes in China. The fertilizer application amount and types have also changed substantially during this period. We use the year-specific statistics of provincial fertilizer application amounts from the China Rural Statistical Yearbook (National Bureau of Statistics (NBSC) 2006–2017), and associated changes in the fractions of synthetic fertilizer types are estimated by the International Fertilizer Association ([www.fertilizer.org](http://www.fertilizer.org)).

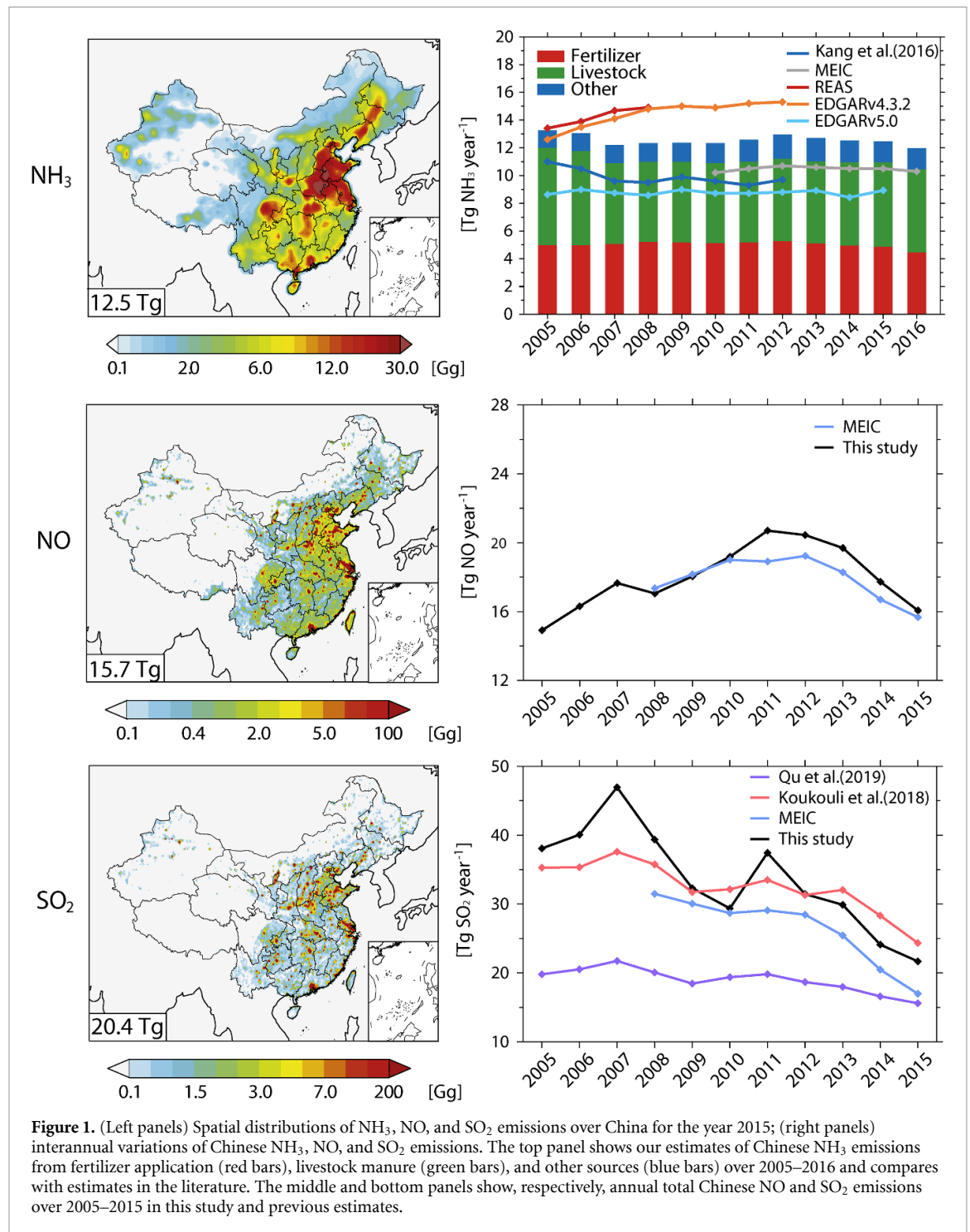
NH<sub>3</sub> emissions from livestock account for six categories of animals, including beef cattle, dairy cows, goat, sheep, pig, and poultry raised in three raising systems: free-range, intensive, and grazing (Zhang *et al* 2018). The most common system in the rural area is free-range, which is the traditional way to raise livestock leading to large NH<sub>3</sub> emissions. The intensive raising system becomes the most popular way near megacities due to its high efficiency and easiness to manage the shelter environment. Grazing mostly occurs in Northwest China. We use the livestock manure mass-flow methodology and emission factors from Huang *et al* (2012), and further consider the meteorology conditions (2 m air temperature and

10 m wind speed) effects on emission factors (Zhang *et al* 2018). The numbers of animals raised in intensive and grazing systems of each province are divided based on the Chinese Animal Husbandry and Veterinary Yearbook (Editorial Committee of China animal husbandry and veterinary Yearbook 2006–2017).

In addition to the agricultural sources, we also include NH<sub>3</sub> emitted from vehicles, biomass burning, residential burning, industry, and waste disposal estimated by Kang *et al* (2016) from 2005 to 2012. To further account for changes in some of these sources over 2013–2016, we assume that NH<sub>3</sub> emissions from vehicle, industry, and residential burning follow the same interannual variations as SO<sub>2</sub> emissions for each source, and apply the corresponding SO<sub>2</sub> emission changes estimated from the MEIC inventory.

Figure 1 shows the spatial distribution of anthropogenic NH<sub>3</sub> emissions over China for the year 2015, and interannual changes in Chinese NH<sub>3</sub> emissions from different sources over 2005–2016. High NH<sub>3</sub> emissions can be found in the eastern China, in particular, over the key regions such as the North China Plain (including Beijing–Tianjin–Hebei (BTH) and surrounding areas), Yangtze River Delta (YRD), Pearl River Delta (PRD), and Sichuan Basin (SCB) (see figure S1 available online at [stacks.iop.org/ERL/16/125004/mmedia](http://stacks.iop.org/ERL/16/125004/mmedia) for their locations). These regions are highly populated and also have intense agricultural activities. The annual total Chinese anthropogenic NH<sub>3</sub> emissions are 12.5 Tg NH<sub>3</sub> in 2015, and range from 12.0–13.3 Tg during 2005–2016, with 37%–42% from fertilizer application and 46%–53% from livestock manure management. The national total NH<sub>3</sub> emissions show relative weak interannual variations, while spatially they generally increase in western China and decrease in eastern China relative to 2005 for both the fertilizer application and livestock sources (figure S2). The increases of NH<sub>3</sub> emissions in western China are largely driven by increasing fertilizer application amount and livestock number, different from those in eastern China and national totals as discussed below.

We find that the national total NH<sub>3</sub> emissions from fertilizer applications are about 5.0 Tg in 2005, increase to 5.3 Tg in 2012, then decrease to 4.5 Tg in 2016 (figure 1). The trend is different from that for the national synthetic fertilizer application amounts, which increase from 24.2 Tg N in 2005 to 27.1 Tg N in 2014, and then decrease to 26.3 Tg N in 2016. Differences in trends of fertilizer use and fertilizer NH<sub>3</sub> can be mainly attributed to the switch of fertilizer type from ammonium bicarbonate (ABC) to urea and compound fertilizer with the latter have lower emission factors (figure S3) as also pointed out by Kang *et al* (2016) and Adalibieke *et al* (2021). NH<sub>3</sub> emissions from livestock are 6.0 Tg in China over 2005–2016, reaching 7.0 Tg in 2005 then dropping to 5.8 Tg in 2007 due to diseases among pigs and increased



costs to raise cattle. The livestock  $\text{NH}_3$  emissions then remained nearly unchanged from 2007 to 2016, although the livestock numbers have increased over this time period, due to a shift of raising systems from free-range to large intensive systems since 2007 (figure S3). Figure 1 also compares our estimates of Chinese  $\text{NH}_3$  emissions estimates with emission estimates in previous studies. Our results are well in the range of the existing inventories, and the interannual variations are similar to estimates of Kang *et al* (2016) and MEIC (Zheng *et al* 2018).

### 3.2. Top-down estimates of Chinese $\text{NO}_x$ and $\text{SO}_2$ emissions during 2005–2015

We use OMI satellite observations of  $\text{NO}_2$  tropospheric columns and  $\text{SO}_2$  PBL columns to constrain the interannual variations of  $\text{NO}_x$  and  $\text{SO}_2$  emissions in China over the period of 2005–2015. We follow the finite-difference mass-balance inversion method from Geddes and Martin (2017). We have conducted two sets of 11 year (2005–2015) GEOS-Chem simulations at the  $2^\circ \times 2.5^\circ$  resolution: one with the Chinese  $\text{SO}_2$  and  $\text{NO}_x$  emissions fixed to

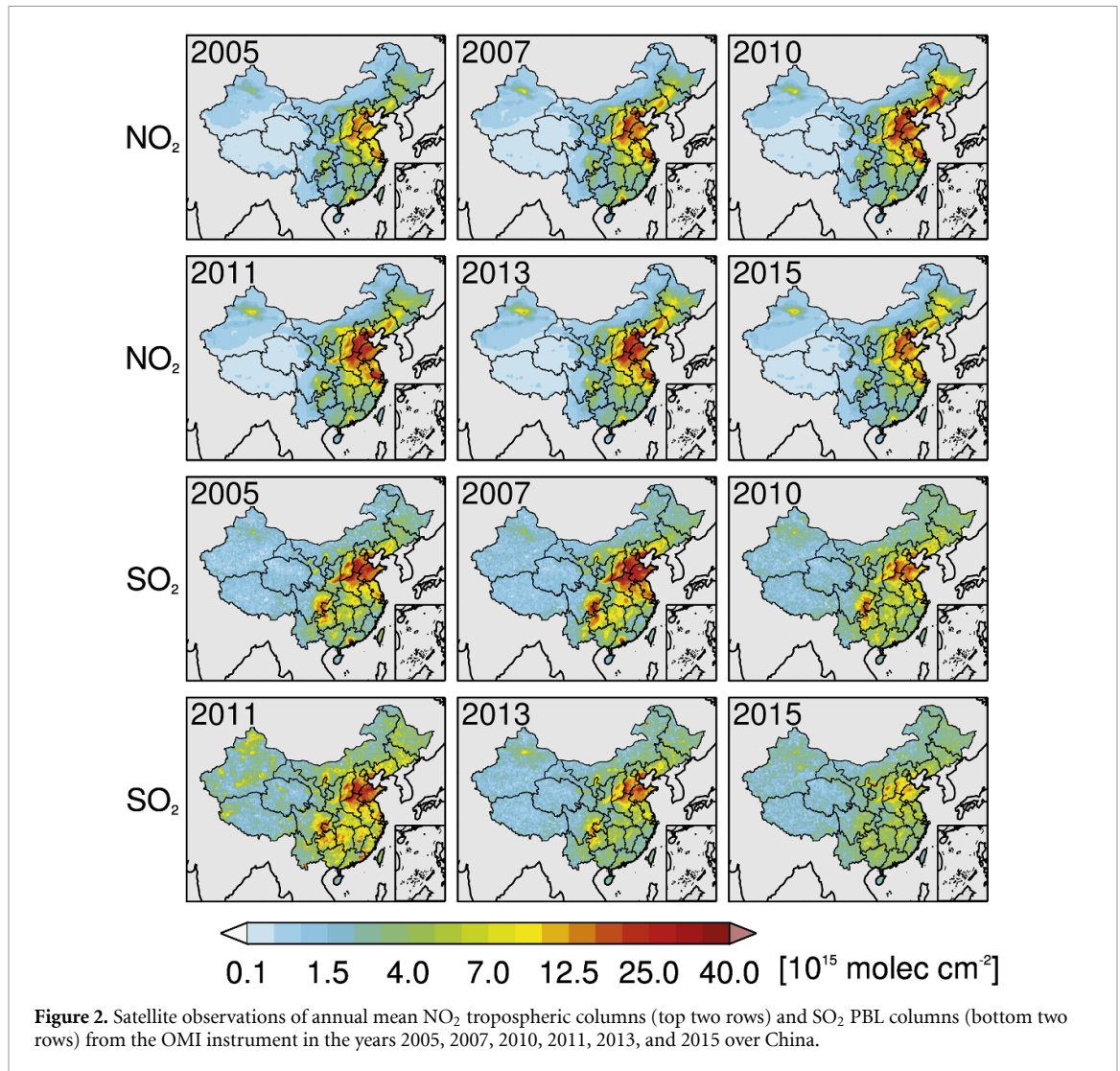


**Figure 2.** Satellite observations of annual mean NO<sub>2</sub> tropospheric columns (top two rows) and SO<sub>2</sub> PBL columns (bottom two rows) from the OMI instrument in the years 2005, 2007, 2010, 2011, 2013, and 2015 over China.

those from the MEIC inventory in the year 2010, and the other applies +30% perturbations on the Chinese SO<sub>2</sub> and NO<sub>x</sub> emissions based on the first simulation setup. We then calculate the changes in simulated NO<sub>2</sub> tropospheric columns and SO<sub>2</sub> PBL columns, and estimate the interannual variations of their emissions for years 2005–2015 using the formula below

$$E_{\text{topdown}} = E_{\text{prior}} \times \left( 1 + \frac{\Delta E}{E_{\text{prior}}} \times \frac{\Omega_{\text{prior}}}{\Delta \Omega} \times \frac{\Omega_{\text{sat}} - \Omega_{\text{prior}}}{\Omega_{\text{prior}}} \right). \quad (1)$$

where  $E_{\text{topdown}}$  is the top-down SO<sub>2</sub> or NO<sub>x</sub> emissions;  $E_{\text{prior}}$  is prior SO<sub>2</sub> or NO<sub>x</sub> emissions based on the 2010 MEIC estimates;  $\Delta E$  is 30% perturbation of  $E_{\text{prior}}$ ;  $\Omega_{\text{prior}}$  is simulated SO<sub>2</sub> or NO<sub>x</sub> columns with prior emissions;  $\Delta \Omega$  is simulated changes of SO<sub>2</sub> or NO<sub>x</sub> columns between prior and 30% perturbation emissions;  $\Omega_{\text{sat}}$  is SO<sub>2</sub> or NO<sub>x</sub> columns observed from OMI. The top-down emissions are calculated monthly and then integrated to annual totals. Here we use the MEIC SO<sub>2</sub> and NO<sub>x</sub> emissions for the year 2010 as the base conditions, and apply the satellite

derived interannual variability over 2005–2015 at each model grid in order to avoid any systematic bias in the satellite observations (Lamsal *et al* 2011, Cooper *et al* 2017, Geddes and Martin 2017).

Figure 2 shows the OMI satellite observations of NO<sub>2</sub> and SO<sub>2</sub> over China in selected 6 years during 2005–2015. Large interannual variations can be seen from these satellite observations, indicating rapid economic development as well as the implementation of emission control measures in China over the time period. Such interannual variations are reflected in the top-down estimates of Chinese NO<sub>x</sub> and SO<sub>2</sub> emissions. Figure 1 also shows the spatial distributions of the top-down Chinese NO<sub>x</sub> (as NO) and SO<sub>2</sub> emissions in 2015 and interannual variations of national totals over 2005–2015 in the context of comparisons with other previous studies. We can see that, according to the OMI satellite observations, NO<sub>x</sub> emissions (as NO) have increased from 14.7 Tg in 2005 to 20.4 Tg in 2011, and then decreased to 15.8 Tg in 2015. The interannual variability of top-down NO<sub>x</sub> emissions are similar to that from the MEIC estimates, although MEIC suggests a later peaking year



and slightly higher emission in 2012 than 2011. The previous studies such as Liu *et al* (2016) and Qu *et al* (2017) also identified that Chinese  $\text{NO}_x$  emissions peaked in 2011 and declined by 21% over 2011–2015 by combining OMI satellite observations and emission inventories. This is consistent with our analysis of 22%  $\text{NO}_x$  emission reduction over 2011–2015, and can be mainly attributed to regulations of power plants and vehicle emissions (Liu *et al* 2016). Over the whole period  $\text{NO}_x$  emissions in China still show an increase of 1.1 Tg (7.5%) in 2015 relative to 2005.

The Chinese  $\text{SO}_2$  emission reductions have occurred earlier due to the application of flue-gas desulfurization devices in power plants since 2006 (Lu *et al* 2010). Our top-down estimates show that Chinese  $\text{SO}_2$  emissions are 46.3 Tg in 2007 and then decrease at a rate of about  $-5.9 \text{ Tg yr}^{-1}$ . The small peak in 2011 can be found in other top-down  $\text{SO}_2$  emission studies (Koukoulis *et al* 2018, Qu *et al* 2019), although our estimates show a much larger interannual variability. The peaks of top-down Chinese  $\text{SO}_2$  emissions in the years 2007 and 2011 mainly reflect the high  $\text{SO}_2$  columns observed from OMI in the two years as can be seen in figure 2. Overall we estimate that  $\text{SO}_2$  emissions in China have decreased from 37.4 Tg in 2005 to 21.0 Tg in 2015 ( $-43.8\%$ ); the trends are similar to the MEIC estimates (Zheng *et al* 2018). It should be noted that the top-down inferred  $\text{NO}_2$  and  $\text{SO}_2$  interannual changes are subject to uncertainties in the OMI retrievals, such as the reduced spatial coverage due to OMI row anomaly since 2007. The OMI products used in this study also treat aerosols implicitly in the retrieval algorithm, which may affect the observed interannual variations over polluted regions with changing aerosol levels (Lin *et al* 2015, Lamsal *et al* 2021).

### 3.3. Impacts of interannual variations of $\text{Nr}$ emissions

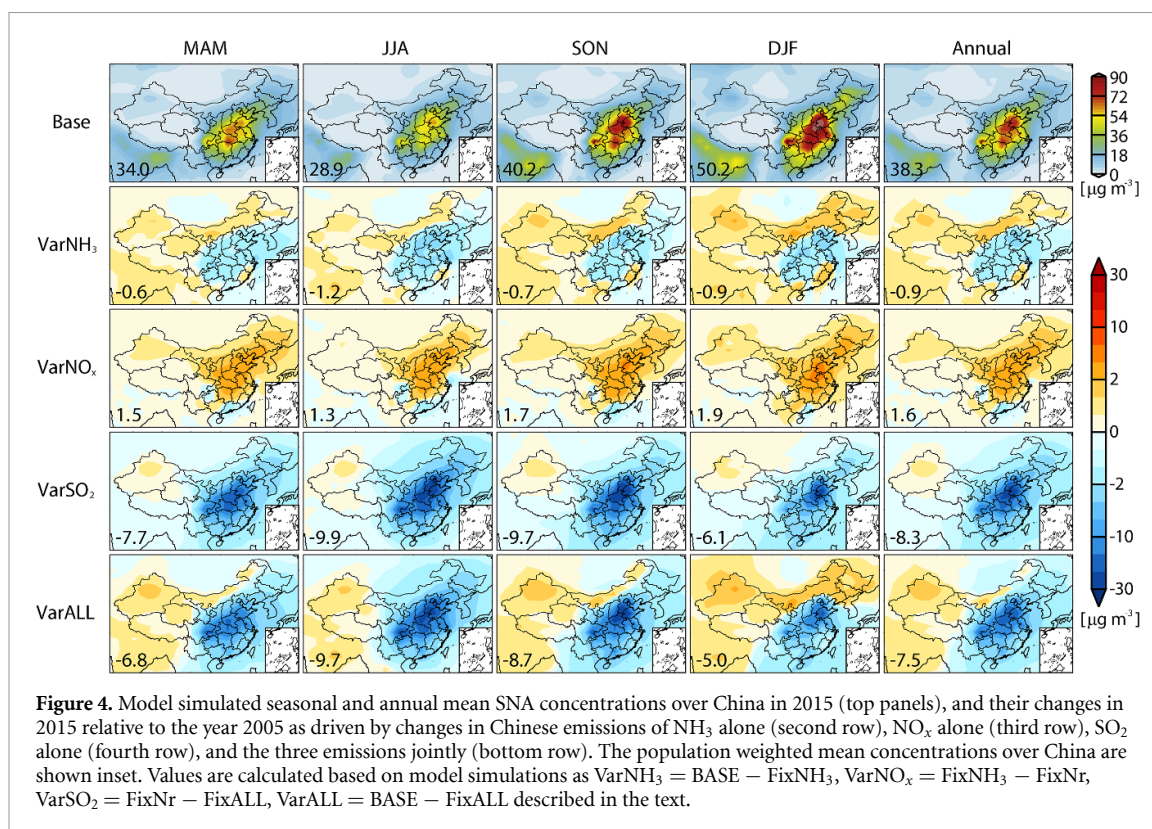
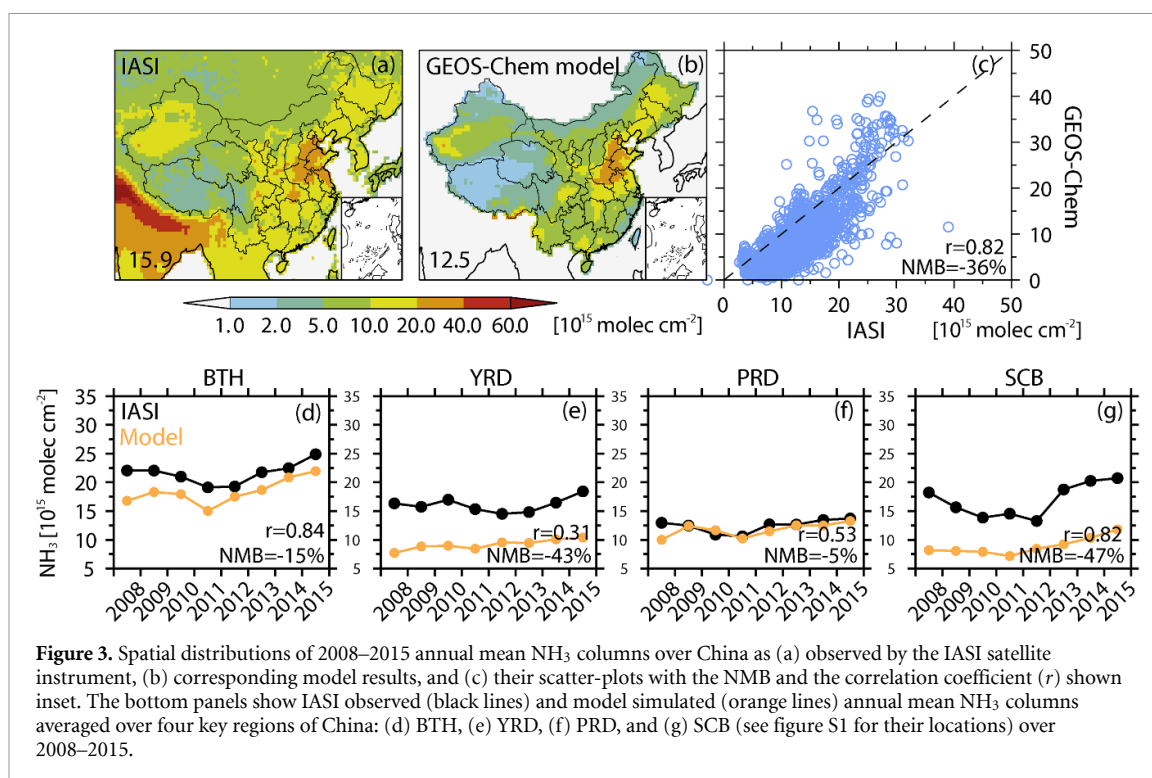
Figures S4–S7 evaluate the BASE simulation with the ensemble of measurements as described above. The BASE model in general reproduces the measured near surface  $\text{NH}_3$  concentrations and nitrogen ( $\text{NH}_4^+$  and  $\text{NO}_3^-$ ) wet deposition fluxes with correlation coefficients of 0.51–0.82 and normalized mean biases (NMBs) within 30%. The model results underestimate the measured  $\text{NH}_3$  concentrations and  $\text{NH}_4^+$  wet deposition fluxes in summer by 41.9% (2015) and 25.0% (2008–2012 average), respectively, likely reflecting that our estimates of Chinese  $\text{NH}_3$  emissions in summer are still biased low. The BASE model results are also in good agreement with the measured surface SNA aerosol concentrations (figure S6). Further evaluations of the model simulated surface  $\text{PM}_{2.5}$  concentrations with CNEMC measurements and satellite products show consistent spatial distributions in eastern China (figure S7).

Figure 3 shows the IASI satellite observed spatial distribution of atmospheric  $\text{NH}_3$  columns and the

corresponding model results averaged over 2008–2015. The comparison of IASI observations and model results shows a high spatial correlation coefficient of 0.82. The model captures the observed high  $\text{NH}_3$  levels over North China, while there is an overall low bias of  $-35.6\%$  relative to the IASI observations, as can be seen from the comparisons over the southern China and western China. In addition to the possible low bias in the  $\text{NH}_3$  emission estimates, IASI  $\text{NH}_3$  measurements may also be biased high due to the relative error weighted method, which tends to give more weight to high values (Van Damme *et al* 2015). We also compare the simulated monthly mean  $\text{NH}_3$  concentrations in January, April, July and October 2005–2015 with AIRS observations at 918 hPa (Warner *et al* 2017) in figure S8. AIRS  $\text{NH}_3$  observations mainly cover the intense agricultural regions of China. We find that compared with the AIRS observations, the seasonal variations of simulated  $\text{NH}_3$  concentrations in China are consistent with a high correlation coefficient (0.85) and a small low bias ( $-5.5\%$ ).

Figure 3 also compares IASI observed and model simulated 2008–2015 interannual variations of  $\text{NH}_3$  columns over the four most densely populated Chinese regions: BTH, YRD, PRD, and SCB. Despite the small interannual variations and decreases since 2012 in the Chinese  $\text{NH}_3$  emissions (figure 1), both IASI satellite observations and model results show increases in atmospheric  $\text{NH}_3$  concentrations since 2011 over the four regions. The BASE model results well capture the IASI observed  $\text{NH}_3$  interannual variation over these regions, although there are considerable underestimates ( $-43\% \sim -47\%$ ) of  $\text{NH}_3$  concentrations over YRD and SCB. Previous studies have reported the increases in atmospheric  $\text{NH}_3$  over the North China (i.e. BTH and surrounding areas) observed by IASI and AIRS, and mainly attributed such  $\text{NH}_3$  increases to  $\text{SO}_2$  emission reductions (Warner *et al* 2017, Liu *et al* 2018a). Here we use our sensitivity simulations (section 2.1) to identify drivers of  $\text{NH}_3$  interannual variations over broader regions of China. We find that over the four regions  $\text{SO}_2$  emission reductions are the dominant factor driving the  $\text{NH}_3$  concentration increases (figure S9). Decreases in  $\text{NO}_x$  emissions since 2011 also show small contributions over BTH and YRD. As explained by Liu *et al* (2018a), reductions in  $\text{SO}_2$  and  $\text{NO}_x$  emissions would lower the formation of SNA and thus enhance the  $\text{NH}_3$  gas-phase partitioning. Changes in the  $\text{NH}_3$  concentration are generally weak except for the sudden drop from 2006 to 2007 over BTH, consistent with the changes in  $\text{NH}_3$  emissions (figure 1).

We now quantify the changes in  $\text{PM}_{2.5}$  air pollution attributable to the interannual changes in  $\text{NH}_3$ ,  $\text{NO}_x$ , and  $\text{SO}_2$  emissions over China. Figure 4 shows the simulated seasonal and annual mean surface SNA aerosol concentrations over China for the year 2015, and also their changes due to the changes in Chinese



$\text{NH}_3$ ,  $\text{NO}_x$ , and  $\text{SO}_2$  emissions from 2005 to 2015. We calculate the national population-weighted SNA concentrations and changes using the population dataset of the Gridded Population of the World version 4 (Center for International Earth Science Information Network (CIESIN) Columbia University 2018).

The national mean population-weighted SNA concentrations are  $38.3 \mu\text{g m}^{-3}$  annually, peaking in winter ( $50.2 \mu\text{g m}^{-3}$ ) and being the lowest in summer ( $28.9 \mu\text{g m}^{-3}$ ). Such strong seasonal variations are largely caused by the higher pollutants' emissions and more frequent stagnant weather conditions



over eastern China in winter than summer, and more effective removal of air pollution by precipitation in summer than winter as well (Liu *et al* 2018b).

Changes in Chinese  $\text{NH}_3$ ,  $\text{NO}_x$ , and  $\text{SO}_2$  emissions in 2015 relative to 2005 have led to large changes in the SNA aerosol concentrations. As shown in figure 4, due to the large reductions in  $\text{SO}_2$  emissions, the annual mean population weighted SNA aerosol concentrations have reduced by  $8.3 \mu\text{g m}^{-3}$ . There is a higher reduction of  $9.9 \mu\text{g m}^{-3}$  in summer than  $6.1 \mu\text{g m}^{-3}$  in winter, reflecting higher efficiency of  $\text{SO}_2$  photochemical oxidation to sulfuric acid in summer. Spatially, in the BTH and SCB, the 2005–2015  $\text{SO}_2$  emission reductions can reduce seasonal and annual mean SNA concentrations by more than  $20 \mu\text{g m}^{-3}$ . Compared to the effects of  $\text{SO}_2$  emission reductions, changes in SNA aerosol concentrations due to 2005–2015  $\text{NH}_3$  and  $\text{NO}_x$  emission changes are weaker. The 2005–2015 reduction of Chinese  $\text{NH}_3$  emissions by 0.8 Tg (−6%) lead to  $-0.9 \mu\text{g m}^{-3}$  changes in SNA, increases of  $\text{NO}$  emissions by 1.1 Tg (7.5%) enhance SNA by  $1.6 \mu\text{g m}^{-3}$ , while changes in Chinese  $\text{SO}_2$  emissions by 16.4 Tg (−48.3%) cause  $-8.3 \mu\text{g m}^{-3}$  reduction. Thus, percentage changes in  $\text{Nr}$  emissions have shown similar efficiency affecting  $\text{PM}_{2.5}$  air pollution than  $\text{SO}_2$  emission changes in China. Together, changes in  $\text{Nr}$  and  $\text{SO}_2$  emissions from 2005 to 2015 could have decreased the annual population weighted  $\text{PM}_{2.5}$  by  $-7.5 \mu\text{g m}^{-3}$  in China ( $-9.7 \mu\text{g m}^{-3}$  in summer and  $-5.0 \mu\text{g m}^{-3}$  in winter).

These changes in the SNA aerosol concentration largely reflect the changes of their precursor emissions, but can also be influenced by the changes in atmospheric oxidants affecting the SNA aerosol formation. For example,  $\text{NO}_x$  emission changes would affect tropospheric ozone concentrations and thus affect the oxidation of  $\text{SO}_2$  to form sulfate aerosol. In turn, changes in aerosol levels would also affect ozone concentrations via aerosol chemistry and photolysis pathways (Li *et al* 2019b). Figure S10 shows the simulated changes in seasonal and annual mean surface ozone concentrations over China caused by changes in Chinese  $\text{NH}_3$ ,  $\text{NO}_x$ , and  $\text{SO}_2$  emissions from 2005 to 2015. Compared with figure 4, the aerosol concentration changes driven by  $\text{NH}_3$  and  $\text{SO}_2$  emission changes tend to be negatively correlated with the ozone concentration changes, likely reflecting the suppression of ozone formation via aerosol radiative effect or the ozone sink via aerosol chemistry. The increases of  $\text{NO}_x$  emissions from 2005 to 2015 could also decrease seasonal mean ozone levels due to titration at night and in winter, except in summer when photochemistry is active. Future work is needed to quantify the interaction of interannual changes in SNA aerosol and ozone concentrations.

Analyzing the interannual variations of emission changes (figure S11), we can see strong influences on the regional SNA aerosol concentration from changes

in Chinese  $\text{NO}_x$  emissions. We estimate that over the study period the Chinese  $\text{NO}_x$  emissions peak in 2011. Increases in  $\text{NO}_x$  emissions from 2005 to 2011 increased the annual mean  $\text{PM}_{2.5}$  concentrations by  $6.5 \mu\text{g m}^{-3}$  in BTH,  $4.6 \mu\text{g m}^{-3}$  in YRD, and  $2.8 \mu\text{g m}^{-3}$  in SCB, offsetting or even exceeding the  $\text{PM}_{2.5}$  decreases due to  $\text{SO}_2$  emission reductions. Estimated changes in  $\text{Nr}$  emissions and their effects on  $\text{PM}_{2.5}$  over PRD are small over this period. Reductions in Chinese  $\text{NO}_x$  emissions after 2011 have accelerated the  $\text{PM}_{2.5}$  decreases. The 2011–2015 Chinese  $\text{NO}_x$  emission reduction reduced regional mean  $\text{PM}_{2.5}$  by  $3.8 \mu\text{g m}^{-3}$  in BTH,  $3.2 \mu\text{g m}^{-3}$  in YRD, and  $2.3 \mu\text{g m}^{-3}$  in SCB. Together changes in Chinese  $\text{Nr}$  and  $\text{SO}_2$  emissions over 2011–2015 have decreased the regional mean  $\text{PM}_{2.5}$  by  $12.5 \mu\text{g m}^{-3}$  in BTH,  $8.8 \mu\text{g m}^{-3}$  in YRD, and  $9.7 \mu\text{g m}^{-3}$  in SCB, with changes in  $\text{Nr}$  emissions contributing 20%–36% of the decreases. According to the CNEMC measurements (figure S7),  $\text{PM}_{2.5}$  concentrations have decreased rapidly in eastern China since 2013 due to stringent air pollution control actions, e.g. decreased by  $\sim 29 \mu\text{g m}^{-3}$  over 2013–2015 in BTH. Our results suggest that  $\sim 40\%$  of the decreases can be attributed to changes in  $\text{Nr}$  and  $\text{SO}_2$  emissions over China.

## 4. Conclusions

We have analyzed the interannual variations of  $\text{Nr}$  ( $\text{NH}_3 + \text{NO}_x$ ) emissions in China over 2005–2015 and quantified their contributions to  $\text{PM}_{2.5}$  air pollution. Satellite observations of  $\text{NH}_3$ ,  $\text{NO}_2$ , and  $\text{SO}_2$  atmospheric concentrations during this time period are used to constrain Chinese  $\text{Nr}$  and  $\text{SO}_2$  emissions. We have applied a bottom-up approach to estimate Chinese  $\text{NH}_3$  emissions, and a top-down approach for  $\text{NO}_x$  and  $\text{SO}_2$  emission estimates. The bottom-up estimates of  $\text{NH}_3$  emissions resolve the interannual variations of agricultural activities such as changes in fertilizer application amounts and types and livestock numbers. We find small interannual changes in the total Chinese anthropogenic  $\text{NH}_3$  emissions, ranging 12.0–13.3 Tg during 2005–2016, with 37%–42% from fertilizer application and 46%–53% from livestock manure management. Although fertilizer and livestock amounts have increased over the time period, the shifts of fertilizer types (from ABC to urea and nitrogen compounds) and livestock raising systems (from free-range to intensive systems) keep the total Chinese  $\text{NH}_3$  emissions relatively stable or even slightly decreasing after 2012.

In contrast to  $\text{NH}_3$ , Chinese  $\text{NO}_x$  and  $\text{SO}_2$  emissions as inferred from the satellite observations show large interannual changes. We estimate that Chinese  $\text{NO}_x$  emissions (as  $\text{NO}$ ) have increased from 14.7 Tg in 2005 to 20.4 Tg in 2011, and then decreased to 15.8 Tg in 2015. Chinese  $\text{SO}_2$  emissions peaked at 46.3 Tg in 2007 and rapidly decreased over 2011–2015, reaching 21.0 Tg in 2015. Based on these

Chinese NH<sub>3</sub>, NO<sub>x</sub>, and SO<sub>2</sub> emissions over 2005–2015, the GEOS-Chem model simulation can well capture the increases of atmospheric NH<sub>3</sub> levels after 2011 in eastern China as observed by the IASI satellite observations (although with some low biases in the model results) and attribute the atmospheric NH<sub>3</sub> increases mainly to the rapid SO<sub>2</sub> emission reductions.

We find that interannual variations of Nr and SO<sub>2</sub> emission changes have strongly influenced the regional SNA components of PM<sub>2.5</sub> in eastern China over 2005–2015. The Chinese NH<sub>3</sub> emission changes in 2015 relative to 2005 (–6%) lead to 0.9 μg m<sup>–3</sup> reductions in the national population weighted mean SNA concentration, compared with an increase of 1.6 μg m<sup>–3</sup> due to 7.5% NO<sub>x</sub> emission increases, and a decrease of 8.3 μg m<sup>–3</sup> due to 48.3% SO<sub>2</sub> emission reductions. The 2011–2015 Chinese NO<sub>x</sub> emission reductions decreased regional mean PM<sub>2.5</sub> by 2.3–3.8 μg m<sup>–3</sup>, also becoming an important driver of recent PM<sub>2.5</sub> air quality improvements. The Chinese air pollution control actions after 2011 have mainly focused on power plant, industry, and transportation sectors that have significantly lowered NO<sub>x</sub> and SO<sub>2</sub> emissions (Zheng et al 2018). Our analyses indicate that strengthening agricultural NH<sub>3</sub> emission reduction can achieve similar effectiveness for further improving PM<sub>2.5</sub> air quality in eastern China.

### Data availability statement

All data that support the findings of this study are available from the corresponding author on reasonable request.

### Acknowledgments

This work is supported by the National Natural Science Foundation of China (NSFC, 41922037), by Grant No. 80NSSC18K0689 (NASA, USA), and also contributes to UNCNET, a project funded under the JPI Urban Europe/China collaboration, Project Nos. 71961137011 (NSFC, China), UMO-2018/29/Z/ST10/02986 (NCN, Poland), and 870234 (FFG, Austria). We thank Dr Juying X. Warner at University of Maryland for providing the AIRS NH<sub>3</sub> observations.

### ORCID iDs

Lin Zhang  <https://orcid.org/0000-0003-2383-8431>  
Xiao Lu  <https://orcid.org/0000-0002-5989-0912>  
Wilfried Winiwarter  <https://orcid.org/0000-0001-7131-1496>

### References

- Adalibieke W, Zhan X, Cui X, Reis S, Winiwarter W and Zhou F 2021 Decoupling between ammonia emission and crop

- production in China due to policy interventions *Glob. Change Biol.* **27** 5877–88
- Bai Z, Ma L, Jin S, Ma W, Velthof G L, Oenema O, Liu L, Chadwick D and Zhang F 2016 Nitrogen, phosphorus, and potassium flows through the manure management chain in China *Environ. Sci. Technol.* **50** 13409–18
- Binkowski F S and Roselle S J 2003 Models-3 community multiscale air quality (CMAQ) model aerosol component 1. Model description *J. Geophys. Res.* **108** 4183
- Boersma K F, Eskes H J, Meijer E W and Kelder H M 2005 Estimates of lightning NO<sub>x</sub> production from GOME satellite observations *Atmos. Chem. Phys.* **5** 2311–31
- Center for International Earth Science Information Network (CIESIN) Columbia University 2018 Gridded population of the world, version 4 (GPWv4): population count, revision 11 (Palisades, NY: NASA Socioeconomic Data and Applications Center (SEDAC)) (available at: <https://doi.org/10.7927/H4JW8BX5>) (Accessed 1 January 2020)
- Ciais P, Sabine C, Bala G, Bopp L, Brovkin V, Canadell J, Chhabra A, DeFries R, Galloway J and Heimann M 2014 Carbon and other biogeochemical cycles, climate change 2013 *The Physical Science Basis Contribution of Working Group I to the Fifth Assessment Report of the Intergovernmental Panel on Climate Change* (Cambridge: Cambridge University Press) pp 465–570
- Cooper M, Martin R V, Padmanabhan A and Henze D K 2017 Comparing mass balance and adjoint methods for inverse modeling of nitrogen dioxide columns for global nitrogen oxide emissions *J. Geophys. Res. Atmos.* **122** 4718–34
- Editorial committee of china animal husbandry and veterinary yearbook 2006–2017 *China Animal Husbandry and Veterinary Yearbook* (Beijing: China Agriculture Press) in Chinese
- Eickenscheidt N, Brumme R and Veldkamp E 2011 Direct contribution of nitrogen deposition to nitrous oxide emissions in a temperate beech and spruce forest—a <sup>15</sup>N tracer study *Biogeosciences* **8** 621–35
- Fountoukis C and Nenes A 2007 ISORROPIA II: a computationally efficient thermodynamic equilibrium model for K<sup>+</sup>–Ca<sup>2+</sup>–Mg<sup>2+</sup>–NH<sub>4</sub><sup>+</sup>–Na<sup>+</sup>–SO<sub>4</sub><sup>2–</sup>–NO<sub>3</sub><sup>–</sup>–Cl<sup>–</sup>–H<sub>2</sub>O aerosols *Atmos. Chem. Phys.* **7** 4639–59
- Galloway J N 2001 Acidification of the world: natural and anthropogenic *Water Air Soil Pollut.* **130** 17–24
- Galloway J N, Aber J D, Erisman J W, Seitzinger S P, Howarth R W, Cowling E B and Cosby B J 2003 The nitrogen cascade *BioScience* **53** 341–56
- Geddes J A and Martin R V 2017 Global deposition of total reactive nitrogen oxides from 1996 to 2014 constrained with satellite observations of NO<sub>2</sub> columns *Atmos. Chem. Phys.* **17** 10071–91
- Guo Y et al 2020 Air quality, nitrogen use efficiency and food security in China are improved by cost-effective agricultural nitrogen management *Nat. Food* **1** 648–58
- Hammer M S et al 2020 Global estimates and long-term trends of fine particulate matter concentrations (1998–2018) *Environ. Sci. Technol.* **54** 7879–90
- Hickman J E, Dammers E, Galy-Lacaux C and van der Werf G R 2018 Satellite evidence of substantial rain-induced soil emissions of ammonia across the Sahel *Atmos. Chem. Phys.* **18** 16713–27
- Hoesly R M et al 2018 Historical (1750–2014) anthropogenic emissions of reactive gases and aerosols from the community emissions data system (CEDS) *Geosci. Model. Dev.* **11** 369–408
- Huang R-J et al 2014 High secondary aerosol contribution to particulate pollution during haze events in China *Nature* **514** 218–22
- Huang X, Song Y, Li M, Li J, Huo Q, Cai X, Zhu T, Hu M and Zhang H 2012 A high-resolution ammonia emission inventory in China *Glob. Biogeochem. Cycles* **26** GB1030
- Kang Y et al 2016 High-resolution ammonia emissions inventories in China from 1980 to 2012 *Atmos. Chem. Phys.* **16** 2043–58

- Kean A J and Harley R A 2000 On-road measurement of ammonia and other motor vehicle exhaust emissions *Environ. Sci. Technol.* **34** 3535–9
- Keller C A, Long M S, Yantosca R M, Da Silva A M, Pawson S and Jacob D J 2014 HEMCO v1.0: a versatile, ESMF-compliant component for calculating emissions in atmospheric models *Geosci. Model. Dev.* **7** 1409–17
- Koukouli M E, Theys N, Ding J, Zyrichidou I, Mijling B, Balis D and van der A R J 2018 Updated SO<sub>2</sub> emission estimates over China using OMI/Aura observations *Atmos. Meas. Tech.* **11** 1817–32
- Krotkov N A, Lamsal L N, Marchenko S V, Celarier E A, Bucsela E J, Swartz W H and Joiner G 2019 OMI/Aura NO<sub>2</sub> Cloud-Screened Total and Tropospheric Column L3 Global Gridded 0.25 degree x 0.25 degree V3, NASA Goddard Space Flight Center, Goddard Earth Sciences Data and Information Services Center (GES DISC) (Accessed 1 January 2020)
- Lamsal L N et al 2021 Ozone monitoring instrument (OMI) Aura nitrogen dioxide standard product version 4.0 with improved surface and cloud treatments *Atmos. Meas. Tech.* **14** 455–79
- Lamsal L N, Martin R V, Padmanabhan A, van Donkelaar A, Zhang Q, Sioris C E, Chance K, Kurosu T P and Newchurch M J 2011 Application of satellite observations for timely updates to global anthropogenic NO<sub>x</sub> emission inventories *Geophys. Res. Lett.* **38** L05810
- Levelt P F, van den Oord G H J, Dobber M R, Malkki A, Visser H, de Vries J, Stammes P, Lundell J O V and Saari H 2006 The ozone monitoring instrument *IEEE Trans. Geosci. Remote Sens.* **44** 1093–101
- Li C, Krotkov N A and Leonard P 2020 OMI/Aura Sulfur Dioxide (SO<sub>2</sub>) Total Column L3 1 day Best Pixel in 0.25 degree × 0.25 degree V3 Greenbelt, MD, USA *Goddard Earth Sciences Data and Information Services Center (GES DISC)* (Accessed 1 January 2020)
- Li H, Cheng J, Zhang Q, Zheng B, Zhang Y, Zheng G and He K 2019a Rapid transition in winter aerosol composition in Beijing from 2014 to 2017: response to clean air actions *Atmos. Chem. Phys.* **19** 11485–99
- Li K, Jacob D J, Liao H, Shen L, Zhang Q and Bates K H 2019b Anthropogenic drivers of 2013–2017 trends in summer surface ozone in China *Proc. Natl Acad. Sci. USA* **116** 422–7
- Li M et al 2017 MIX: a mosaic Asian anthropogenic emission inventory under the international collaboration framework of the MICS-Asia and HTAP *Atmos. Chem. Phys.* **17** 935–63
- Lin J-T, Liu M-Y, Xin J-Y, Boersma K F, Spurr R, Martin R and Zhang Q 2015 Influence of aerosols and surface reflectance on satellite NO<sub>2</sub> retrieval: seasonal and spatial characteristics and implications for NO<sub>x</sub> emission constraints *Atmos. Chem. Phys.* **15** 11217–41
- Liu F, Zhang Q, van der A R J, Zheng B, Tong D, Yan L, Zheng Y and He K 2016 Recent reduction in NO<sub>x</sub> emissions over China: synthesis of satellite observations and emission inventories *Environ. Res. Lett.* **11** 114002
- Liu H, Jacob D J, Bey I and Yantosca R M 2001 Constraints from <sup>210</sup>Pb and <sup>7</sup>Be on wet deposition and transport in a global three-dimensional chemical tracer model driven by assimilated meteorological fields *J. Geophys. Res. Atmos.* **106** 12109–28
- Liu M et al 2018a Rapid SO<sub>2</sub> emission reductions significantly increase tropospheric ammonia concentrations over the North China plain *Atmos. Chem. Phys.* **18** 17933–43
- Liu M et al 2019 Ammonia emission control in China would mitigate haze pollution and nitrogen deposition, but worsen acid rain *Proc. Natl Acad. Sci. USA* **116** 7760–5
- Liu X et al 2013 Enhanced nitrogen deposition over China *Nature* **494** 459–62
- Liu Z et al 2018b Characteristics of PM<sub>2.5</sub> mass concentrations and chemical species in urban and background areas of China: emerging results from the CARE-China network *Atmos. Chem. Phys.* **18** 8849–71
- Liu Z, Zhou M, Chen Y, Chen D, Pan Y, Song T, Ji D, Chen Q and Zhang L 2021 The nonlinear response of fine particulate matter pollution to ammonia emission reductions in North China *Environ. Res. Lett.* **16** 034014
- Lu X et al 2021 The underappreciated role of agricultural soil nitrogen oxide emissions in ozone pollution regulation in North China *Nat. Commun.* **12** 5021
- Lu Z, Streets D G, Zhang Q, Wang S, Carmichael G R, Cheng Y F, Wei C, Chin M, Diehl T and Tan Q 2010 Sulfur dioxide emissions in China and sulfur trends in East Asia since 2000 *Atmos. Chem. Phys.* **10** 6311–31
- Mao J et al 2010 Chemistry of hydrogen oxide radicals (HO<sub>x</sub>) in the arctic troposphere in spring *Atmos. Chem. Phys.* **10** 5823–38
- National Bureau of Statistics (NBSC) 2006–2017 *China Rural Statistical Yearbook* (Beijing: China Statistics) (in Chinese)
- Pan Y P, Wang Y S, Tang G Q and Wu D 2012 Wet and dry deposition of atmospheric nitrogen at ten sites in Northern China *Atmos. Chem. Phys.* **12** 6515–35
- Pan Y et al 2018 Identifying ammonia hotspots in China using a national observation network *Environ. Sci. Technol.* **52** 3926–34
- Park R J, Jacob D J, Field B D and Yantosca R M 2004 Natural and transboundary pollution influences on sulfate-nitrate-ammonium aerosols in the United States: implications for policy *J. Geophys. Res.* **109** D15204
- Paulot F, Jacob D J, Pinder R W, Bash J O, Travis K and Henze D K 2014 Ammonia emissions in the United States, European Union, and China derived by high-resolution inversion of ammonium wet deposition data: interpretation with a new agricultural emissions inventory (MASAGE\_NH<sub>3</sub>) *J. Geophys. Res. Atmos.* **119** 4343–64
- Pilegaard K et al 2006 Factors controlling regional differences in forest soil emission of nitrogen oxides (NO and N<sub>2</sub>O) *Biogeosciences* **3** 651–61
- Qu Z et al 2019 SO<sub>2</sub> emission estimates using OMI SO<sub>2</sub> retrievals for 2005–2017 *J. Geophys. Res. Atmos.* **124** 8336–59
- Qu Z, Wang J and Keller M 2017 Monthly top-down NO<sub>x</sub> emissions for China (2005–2012): a hybrid inversion method and trend analysis *J. Geophys. Res. Atmos.* **122** 4600–25
- Sha Z, Liu H, Wang J, Ma X, Liu X and Misselbrook T 2021 Improved soil-crop system management aids in NH<sub>3</sub> emission mitigation in China *Environ. Pollut.* **289** 117844
- Shao J et al 2019 Heterogeneous sulfate aerosol formation mechanisms during wintertime Chinese haze events: air quality model assessment using observations of sulfate oxygen isotopes in Beijing *Atmos. Chem. Phys.* **19** 6107–23
- Sun K et al 2017 Vehicle emissions as an important urban ammonia source in the United States and China *Environ. Sci. Technol.* **51** 2472–81
- The acid deposition monitoring network in East Asia (available at: [www.eanet.asia/](http://www.eanet.asia/)) (Accessed 1 January 2020)
- Van Damme M et al 2015 Towards validation of ammonia (NH<sub>3</sub>) measurements from the IASI satellite *Atmos. Meas. Tech.* **8** 1575–91
- Van Damme M, Clarisse L, Heald C L, Hurtmans D, Ngadi Y, Clerbaux C, Dolman A J, Erisman J W and Coheur P F 2014 Global distributions, time series and error characterization of atmospheric ammonia (NH<sub>3</sub>) from IASI satellite observations *Atmos. Chem. Phys.* **14** 2905–22
- Van Damme M, Whitburn S, Clarisse L, Clerbaux C, Hurtmans D and Coheur P F 2017 Version 2 of the IASI NH<sub>3</sub> neural network retrieval algorithm: near-real-time and reanalysed datasets *Atmos. Meas. Tech.* **10** 4905–14
- Vitousek P M, Hättenschwiler S, Olander L and Allison S 2002 Nitrogen and Nature *AMBIO A J. Hum. Environ.* **31** 97–101
- van der A R J, Mijling B, Ding J, Koukouli M E, Liu F, Li Q, Mao H and Theys N 2017 Cleaning up the air: effectiveness of air quality policy for SO<sub>2</sub> and NO<sub>x</sub> emissions in China *Atmos. Chem. Phys.* **17** 1775–89
- Wang S, Xing J, Jang C, Zhu Y, Fu J S and Hao J 2011 Impact assessment of ammonia emissions on inorganic aerosols in

- East China using response surface modeling technique  
*Environ. Sci. Technol.* **45** 9293–300
- Wang Y, Zhang Q Q, He K, Zhang Q and Chai L 2013 Sulfate-nitrate-ammonium aerosols over China: response to 2000–2015 emission changes of sulfur dioxide, nitrogen oxides, and ammonia *Atmos. Chem. Phys.* **13** 2635–52
- Warner J X, Dickerson R R, Wei Z, Strow L L, Wang Y and Liang Q 2017 Increased atmospheric ammonia over the world's major agricultural areas detected from space *Geophys. Res. Lett.* **44** 2875–84
- Warner J X, Wei Z, Strow L L, Dickerson R R and Nowak J B 2016 The global tropospheric ammonia distribution as seen in the 13-year AIRS measurement record *Atmos. Chem. Phys.* **16** 5467–79
- Wesely M L 1989 Parameterization of surface resistances to gaseous dry deposition in regional-scale numerical models *Atmos. Environ.* **23** 1293–304
- Xu W *et al* 2015 Quantifying atmospheric nitrogen deposition through a nationwide monitoring network across China *Atmos. Chem. Phys.* **15** 12345–60
- Zhai S *et al* 2021 Control of particulate nitrate pollution in China *Nat. Geosci.* **14** 389–95
- Zhang L *et al* 2018 Agricultural ammonia emissions in China: reconciling bottom-up and top-down estimates *Atmos. Chem. Phys.* **18** 339–55
- Zhang L, Gong S, Padro J and Barrie L 2001 A size-segregated particle dry deposition scheme for an atmospheric aerosol module *Atmos. Environ.* **35** 549–60
- Zhang L, Liu L, Zhao Y, Gong S, Zhang X, Henze D K, Capps S L, Fu T-M, Zhang Q and Wang Y 2015 Source attribution of particulate matter pollution over North China with the adjoint method *Environ. Res. Lett.* **10** 084011
- Zhang L, Shao J, Lu X, Zhao Y, Hu Y, Henze D K, Liao H, Gong S and Zhang Q 2016 Sources and processes affecting fine particulate matter pollution over north China: an adjoint analysis of the Beijing APEC period *Environ. Sci. Technol.* **50** 8731–40
- Zhang Q *et al* 2019 Drivers of improved PM<sub>2.5</sub> air quality in China from 2013 to 2017 *Proc. Natl Acad. Sci. USA* **116** 24463–9
- Zhang X Y, Wang Y Q, Niu T, Zhang X C, Gong S L, Zhang Y M and Sun J Y 2012 Atmospheric aerosol compositions in China: spatial/temporal variability, chemical signature, regional haze distribution and comparisons with global aerosols *Atmos. Chem. Phys.* **12** 779–99
- Zhao Y, Zhang L, Pan Y, Wang Y, Paulot F and Henze D K 2015 Atmospheric nitrogen deposition to the northwestern Pacific: seasonal variation and source attribution *Atmos. Chem. Phys.* **15** 10905–24
- Zheng B *et al* 2018 Trends in China's anthropogenic emissions since 2010 as the consequence of clean air actions *Atmos. Chem. Phys.* **18** 14095–111